Received: 28 May 2017 | Revised: 14 July 2017 | Accepted: 17 July 2017

DOI: 10.1002/aoc.4029

FULL PAPER

WILEY Applied Organometallic Chemistry

Green bio-based synthesis of Fe_2O_3@SiO_2-IL/Ag hollow spheres and their catalytic utility for ultrasonic-assisted synthesis of propargylamines and benzo[*b*]furans

Samahe Sadjadi[1] | Majid M. Heravi[2] | Masoumeh Malmir[2]

[1] Gas Conversion Department, Faculty of Petrochemicals, Iran Polymer and Petrochemicals Institute, PO Box 14975-112, Tehran, Iran

[2] Department of Chemistry, School of Science, Alzahra University, PO Box 1993891176, Vanak, Tehran, Iran

Correspondence
Samahe Sadjadi, Gas Conversion Department, Faculty of Petrochemicals, Iran Polymer and Petrochemicals Institute, PO Box 14975-112, Tehran, Iran.
Email: samahesadjadi@yahoo.com
Majid Heravi, Department of Chemistry, School of Science, Alzahra University, PO Box 1993891176, Vanak, Tehran, Iran.
Email: mmh1331@yahoo.com

A novel magnetic hybrid system containing nano-magnetic Fe_2O_3 hollow spheres, silica shell, [pmim]Cl ionic liquid and silver nanoparticles was synthesized and characterized. The silver nanoparticles were prepared via biosynthesis using *Achillea millefolium* flower as reducing and stabilizing agent. The hybrid system was successfully used as an efficient and reusable catalyst for promoting green ultrasonic-assisted A^3 and KA^2 coupling reactions as well as benzo[*b*]furan synthesis. It was found that decoration of the magnetic core with non-magnetic moieties decreased the maximum saturation magnetization. However, the catalyst was still superparamagnetic and could be simply separated from the reaction mixture using an external magnet. The heterogeneous nature of the catalyst was also confirmed by studying its reusability and stability and the leaching of silver. Use of aqueous media, high yields, short reaction times, broad substrate tolerance and low required amount of catalyst are the merits of this protocol.

KEYWORDS
A^3 and KA^2 coupling reactions, benzo[*b*]furan, biosynthesis, magnetic nanoparticles, propargylamine

1 | INTRODUCTION

Core–shell magnetic nanoparticles exhibit exceptional properties including high surface area, remarkable magnetic susceptibility and coercivity.[1] They have found various applications in a diverse range of research fields such as sensors, drug delivery, diagnosis, immobilization of biologically active species, magnetic separation and most importantly catalysis.[2–4] Utilization of magnetic nanoparticles in catalysis facilitates the recovery and separation of the catalyst and makes the procedure cost-effective and clean.[5–7] To date, various magnetic nanoparticles and magnetic core–shell hybrids with a variety of sizes, morphologies and magnetic properties have been developed. In this context, hollow magnetic nanoparticles are attracting increasing attention due to their outstanding features such as tiny particle sizes, high surface areas and low densities. In this regard, the most challenging issue is the aggregations of hollow magnetic nanoparticles, which can be suppressed by surface modification and introduction of organic functionalities.[6]

In the last decade, multicomponent reactions have received considerable attention as an effective way to achieve molecular complexity through simple and readily available starting materials in one-pot procedures.[8] As important starting materials, acetylenes have a diverse range of applications in multicomponent reactions and organic transformations, such as click reactions, Suzuki, Heck and Sonogashira reactions, A^3 coupling reactions, etc. Among organic reactions, an A^3 coupling reaction, a three-component coupling reaction of aldehydes, amines and alkynes, is a promising pathway for the synthesis of propargylamines. Propargylamines are considered as

important intermediates with utility for the synthesis of more complicated chemicals including biologically attractive nitrogen-containing compounds such as herbicides, fungicides, restricted peptide isosteres, pyrroles, indolizines, oxotremorine analogues as well as natural products.[9–13] Generally, in the literature, diverse methodologies using various catalysts such Zn-, Ir-, Ni-, Cu-, Ag-, Au- and Fe-based catalysts have been reported for promoting A^3 coupling reactions.[9,14–16] In this line, some novel catalysts including sulfonate-based Cu(I) metal–organic frameworks,[17] Cu_2O/nano-$CuFe_2O_4$,[18] Cu(II) Schiff base complex immobilized on graphene oxide,[19] CuI catalysts supported on protonated trititanate nanotubes,[20] copper nanoparticles supported on starch microparticles,[21] Cu(II) chloride,[22] magnetic Fe_3O_4@Au nanoparticles[23] and magnetically separable CuO nanoparticles supported on graphene oxide[24] have been recently introduced.

The main challenges in most of these previously reported protocols are the need for high temperature, long reaction times, inert atmosphere, some toxic solvents or costly media such as ionic liquids or transition or precious metals and the homogeneous nature of the catalyst.[25] Therefore, developing a novel, efficient, rapid and green protocol for the synthesis of propargylamines is of great importance.

A^3 coupling reactions can be exploited for the synthesis of benzofurans. These heterocycles are important pharmacophores and clinically applied drugs, which are prepared via A^3 coupling reaction followed by intramolecular cyclizations.[26,27] In this context various catalysts such as CuI nanoparticles[28,29] and hierarchically porous sphere-like copper oxide[30] can be applied. Therefore, designing novel and efficient methods for the preparation of these compounds is of great interest.

Utilization of ultrasonic irradiation as an efficient, green and clean unconventional procedure for promoting organic transformations is a growing field in green chemistry.[31,32] In ultrasonic chemistry, the cavitation effect is of great influence. Such ultrasonic irradiation can result in the formation of high local temperatures and pressures inside bubbles which accelerate mass transfer and turbulent flow in the liquid.[32] Ultrasonic-assisted procedures benefit from various advantageous including simplicity, rapidness, minimization of waste, high yields and purity of products.

In continuation of systematic research on the development of efficient and heterogeneous nanocatalysts[33–37] for promoting various chemical transformations and introducing green and cost-effective protocols,[6,33,38] herein we report a novel magnetic hybrid catalyst, h-Fe_2O_3@SiO_2-IL/Ag, prepared through the synthesis of nanomagnetic Fe_2O_3 hollow spheres followed by coating them with a silica shell, conjugation of [pmim]Cl ionic liquid and immobilization of Ag(0) nanoparticles via a biosynthetic approach. The catalytic utility of the novel catalyst for promoting green and ultrasonic-assisted synthesis of propargylamines from reaction of amine, phenylacetylene and aldehyde (Scheme 1a) as well as the synthesis of benzo[*b*]furans through reaction of amine, phenylacetylene and salicylaldehydes (Scheme 1b) is studied. Furthermore, the reusability and stability of the catalyst as well as silver leaching are investigated to elucidate the nature of the catalysis. Notably, the comparison of the performance of h-Fe_2O_3@SiO_2-IL/Ag with some of the previously reported ones was accomplished.

2 | EXPERIMENTAL

2.1 | Materials and instrumentation

All chemicals, including $FeCl_3{\cdot}6H_2O$, sodium acetate trihydrate, trisodium citrate dihydrate, tetraethyl orthosilicate (TEOS), toluene, acetone, ethanol, ethylene glycol, urea, $AgNO_3$, $NH_3{\cdot}H_2O$, aldehydes, amines and phenylacetylene, were of analytical grade, purchased from Sigma-Aldrich and used without further purification. The progress of all organic reactions was monitored using TLC with commercial aluminium-backed plates of silica gel 60 F254, using UV light. Melting points were determined in open capillaries using an Electrothermal 9100 without further corrections. ^{1}H NMR spectra were obtained using a Bruker DRX-400 spectrometer at 400 and 100 MHz, Supporting information.

The catalyst was characterized using various techniques including scanning electron microscopy (SEM)/energy-dispersive X-ray (EDX) analysis, Fourier

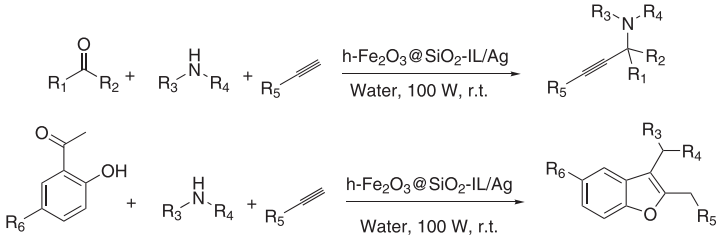

SCHEME 1 A^3 and KA^2 coupling reactions for the synthesis of (a) propargylamines and (b) benzo[*b*]furans

transform infrared (FT-IR) spectroscopy, vibrating sample magnetometry (VSM), X-ray diffraction (XRD), thermogravimetric analysis (TGA), Brunauer–Emmett–Teller (BET) measurements and inductively coupled plasma atomic emission spectrometry (ICP-AES). SEM/EDX images were obtained with a Tescan instrument, using Au-coated samples and an acceleration voltage of 20 kV. FT-IR spectra were recorded with a PerkinElmer Spectrum 65 instrument. BET analysis was carried out using a Belsorp Mini II instrument. The degassing process was performed by heating the catalyst at 423 K for 3 h. Room temperature powder XRD patterns were obtained using a Siemens D5000 with Cu Kα radiation from a sealed tube. TGA was carried out using a Mettler Toledo instrument with a heating rate of 10 °C min^{-1} from 50 to 800 °C under nitrogen atmosphere. The magnetic properties of the catalyst and h-Fe_2O_3 were characterized using VSM (Lakeshore7407) at room temperature. The ultrasonic apparatus used for in this work was a Bandelin HD 3200 with output power of 150 W and tip TT13.

2.2 | Synthesis of Nanomagnetic Fe_2O_3 hollow spheres

The nanomagnetic Fe_2O_3 hollow spheres (h-Fe_2O_3) were prepared via a previously reported solvothermal process.[6] Briefly, $FeCl_3{\cdot}6H_2O$ (5 mmol) was dissolved in ethylene glycol (70 ml) in a flask. Then, a mixture of trisodium citrate dihydrate (1.5 mmol), sodium acetate (30 mmol) and urea (17 mmol) was added to the solution. Subsequently, the brown mixture was stirred energetically for 1 h, transferred to a Teflon-lined stainless steel autoclave (150 ml capacity) and kept at 220 °C overnight. Upon completion of the process, the reactor was cooled and the resulting product (**1**; Figure 1a) was filtered, washed three times with EtOH–H_2O and dried at 80 °C for 24 h in an oven.

2.3 | Synthesis of h-Fe_2O_3@SiO_2 Core–Shell

The preparation of h-Fe_2O_3@SiO_2 was performed according to a previously reported method[39] with slight modification. Typically, h-Fe_2O_3 (1 g) was dispersed in a mixture of ethanol (50 ml), deionized water (20 ml) and NH_3 (6 ml). Notably, the pH of the resulting mixture was kept at *ca* 11. Subsequently, to achieve high dispersion, the mixture was sonicated at ambient temperature for 0.5 h. Then, TEOS (2 g) was added slowly into the obtained light brown mixture, which was continuously stirred at room temperature for 12 h in air. At the end of the process, the as-prepared h-Fe_2O_3@SiO_2 core–shell (**2**; Figure 1b) was simply collected using an external magnet. To remove the unreacted silica and purify h-Fe_2O_3@SiO_2 core–shell, it was washed three times with EtOH–H_2O and then dried at 80 °C for 12 h in an oven.

2.4 | Synthesis of 1-methyl-3-(trimethoxysilylpropyl)imidazolium chloride ([pmim]cl)

[pmim]Cl was prepared according to the literature.[40] Typically, *N*-methylimidazole (1 mol) was mixed with (3-chloropropyl)trimethoxysilane (1 mol) at room temperature. Then, the resulting mixture was refluxed at 95 °C overnight. Upon completion of the reaction, the mixture was cooled to ambient temperature. The pure [pmim]Cl was obtained after washing with diethyl ether and drying under vacuum at 40 °C.

2.5 | Synthesis of h-Fe_2O_3@SiO_2-IL

To synthesize h-Fe_2O_3@SiO_2-IL (Figure 1c), **2** (2 g) was dispersed in EtOH (250 ml) and then sonicated for 0.5 h. After that, the suspension was stirred vigorously at room temperature in a round-bottom flask. Subsequently, a solution of [pmim]Cl (6 g) in deionized water (100 ml) and $NH_3{\cdot}H_2O$ (1 ml) was introduced to the suspension and the resulting mixture was stirred for 36 h. After completion of the reaction, the resulting product was magnetically collected and washed three times with EtOH–H_2O. The wet powder was then dissolved in 50 ml of methanol and stirred at room temperature for 0.5 h. During the stirring process, 50 ml of diethyl ether was added into the flask. Then, the final product (**3**) was magnetically collected, washed three times with diethyl ether and dried at 80 °C for 12 h in an oven.

2.6 | Preparation of *Achillea millefolium* flowering plant extracts

Fresh leaves of *A. millefolium* were collected from Alborz city, Iran. Initially, the *A. millefolium* flowers (2 g) were crushed in a porcelain mortar. The obtained powder was then suspended in deionized water (100 ml) and boiled at 80 °C for 1 h. The concentrated extract (**4**; Figure 1e) was then cooled and filtered.

2.7 | Loading of ag nanoparticles on h-Fe_2O_3@SiO_2-IL: Synthesis of h-Fe_2O_3@SiO_2-IL/Ag

Synthesis and immobilization of silver nanoparticles were achieved through the following procedure. Initially, h-Fe_2O_3@SiO_2-IL (1 g) was introduced into a solution of $Ag(NH_3)_2NO_3$ (0.1 g) in deionized water (20 ml). The

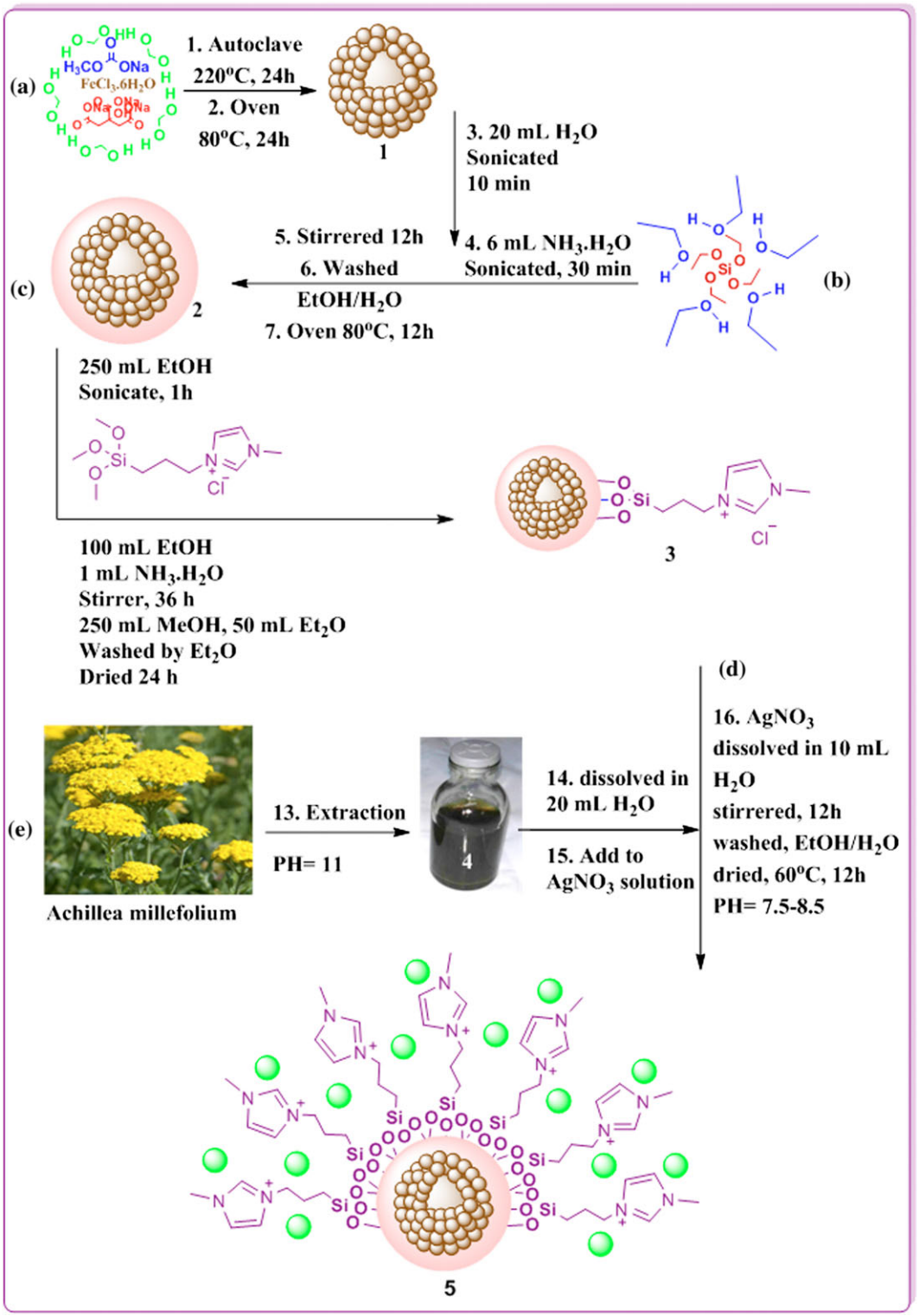

FIGURE 1 Possible formation process of h-Fe_2O_3@SiO_2-IL/Ag hollow spheres

resulting mixture was then stirred at room temperature for 0.5 h. It is postulated that electrostatic attraction kept the $[Ag(NH_3)_2]^+$ ions adsorbed on the surfaces of h-Fe_2O_3@SiO_2-IL. To reduce the silver salt and furnish Ag(0) nanoparticles, *A. millefolium* extract was employed as a reducing and stabilizing agent. Typically, the fresh extract (2 ml) was added into the suspension. The mixture was then stirred for 12 h. Finally, the product (**5**; Figure 1d) was magnetically collected, washed three times with EtOH–H_2O and dried at 60 °C for 12 h. The general synthetic procedure of h-Fe_2O_3@SiO_2-IL/Ag is illustrated in Figure 1.

2.8 | General procedure for synthesis of Propargylamine

A catalytic amount of nanomagnetic h-Fe_2O_3@SiO_2-IL/Ag (25 mg) was added to a mixture of amine (1.0 equiv.), acetylene (1.1 equiv.) and aldehyde or ketone (1.0 equiv.) in water (10 ml). The reaction mixture was then ultrasonicated at 100 W for 10 min (the progress of the reaction was monitored by TLC). At the end of the reaction, the mixture was cooled to room temperature and the mixture was diluted with hot ethanol (10 ml). The separation of the catalyst was easily performed using an external magnet. Notably, the recovered catalyst could be washed with ethanol and reused after dying for subsequent reaction runs. The purification of propargylamine was accomplished by recrystallization from hot ethanol.

2.9 | General procedure for synthesis of 2,3-Disubstituted Benzofurans

To a solution of salicylaldehyde (2 equiv.), acetylene (1.5 equiv.) and amine (1 equiv.) in 5 ml of water, NaOH (1.0 equiv.) and h-Fe_2O_3@SiO_2-IL/Ag (25 mg) were added. Then, the resulting mixture was subjected to ultrasonic irradiation at a power of 100 W. The progress of the reaction was continuously monitored by TLC. After completion of the reaction, the mixture was cooled to room temperature and the catalyst was magnetically separated. After that, the solution was extracted using ethyl acetate (5 ml). The combined organic layer was diluted with hot ethanol to give the crude product. The diluted solution was purified by recrystallization using ethanol to afford pure benzofurans.

3 | RESULTS AND DISCUSSION

3.1 | Catalyst characterization

Initially, the morphology of h-Fe_2O_3@SiO_2 was studied using SEM. It can be clearly seen from Figure 2(a) that h-Fe_2O_3@SiO_2 particles exhibited spherical morphology. Interestingly, h-Fe_2O_3@SiO_2-IL/Ag also possessed spherical morphology indicating that combining IL and Ag(0) nanoparticles did not induce considerable morphology change and the spherical morphology of h-Fe_2O_3@SiO_2 was preserved. Notably, in h-Fe_2O_3@SiO_2-IL/Ag small

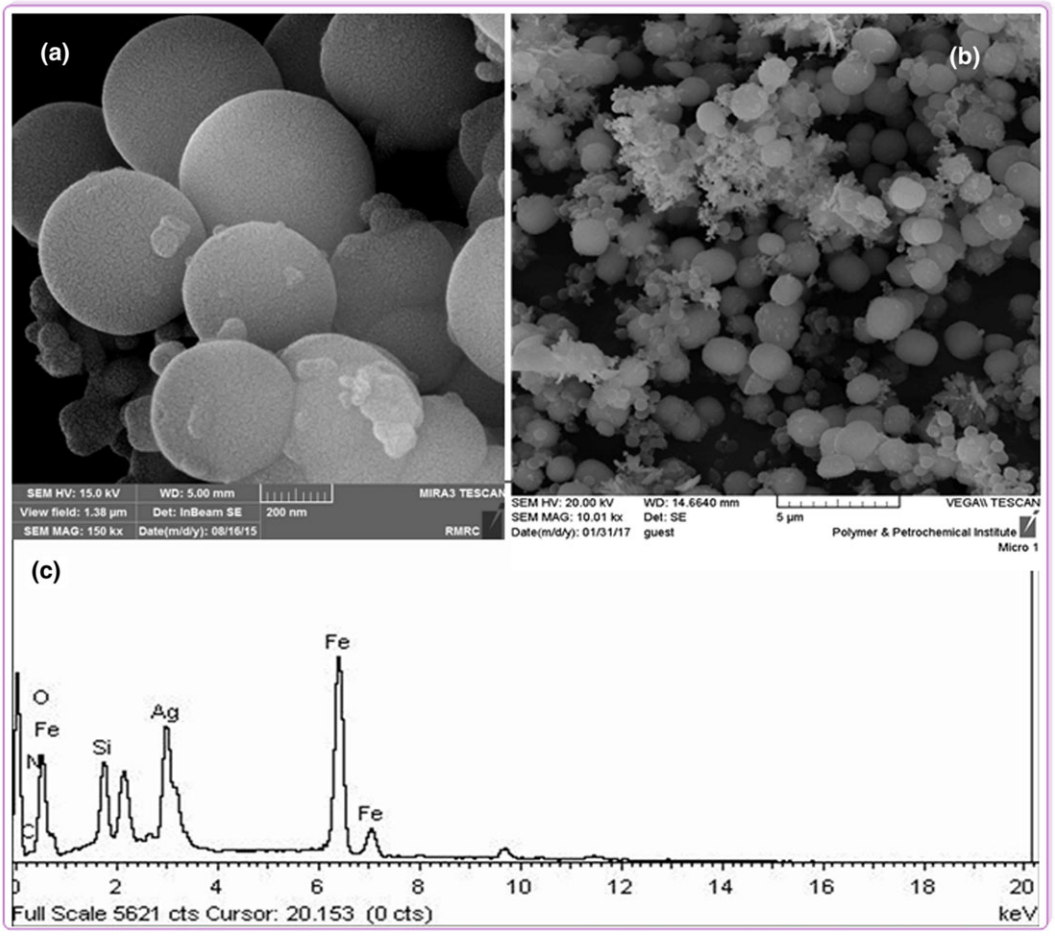

FIGURE 2 (a) SEM image of h-Fe_2O_3@SiO_2 and (b) SEM image of h-Fe_2O_3@SiO_2-IL/ag. (c) EDX analysis of h-Fe_2O_3@SiO_2-IL/Ag

non-spherical aggregates can also be observed, which can be attributed to the unattached IL and the organic compounds of the flower extract (Figure 2b).

The h-Fe_2O_3@SiO_2-IL/Ag catalyst was also investigated using EDX analysis (Figure 2c). The formation of magnetic nanoparticles can be confirmed by observation of signals of Fe and O atoms. Notably, the Fe_2O_3 magnetic nanoparticles were also confirmed using more precise techniques such as XRD. The presence of Si and O atoms can be indicative of the formation of SiO_2 shell. The appearance of N, Si and C signals in EDX analysis can be assigned to the presence of IL. Finally, observation of Ag signal can establish the immobilization of Ag(0) nanoparticles.

The elemental mapping analysis of the catalyst is depicted in Figure 3. The good dispersion of Si species can confirm the formation of the silica shell. Moreover, the abundance of silver species indicated the efficiency of IL for anchoring the silver species. Notably, Ag is distributed almost uniformly on the surface of the catalyst.

The FT-IR spectrum of h-Fe_2O_3@SiO_2-CD/Ag is depicted in Figure 4. This spectrum clearly exhibited the characteristic bands of silica shell, i.e. the bands at 1089 cm^{-1}, which can be assigned to Si—O stretching, and the bands at 980 and 810 cm^{-1}, which can be attributed to the bending vibrations of the Si—O—Si bond.[1] Moreover, Fe—O stretching vibration can be confirmed by observing strong absorption bands at

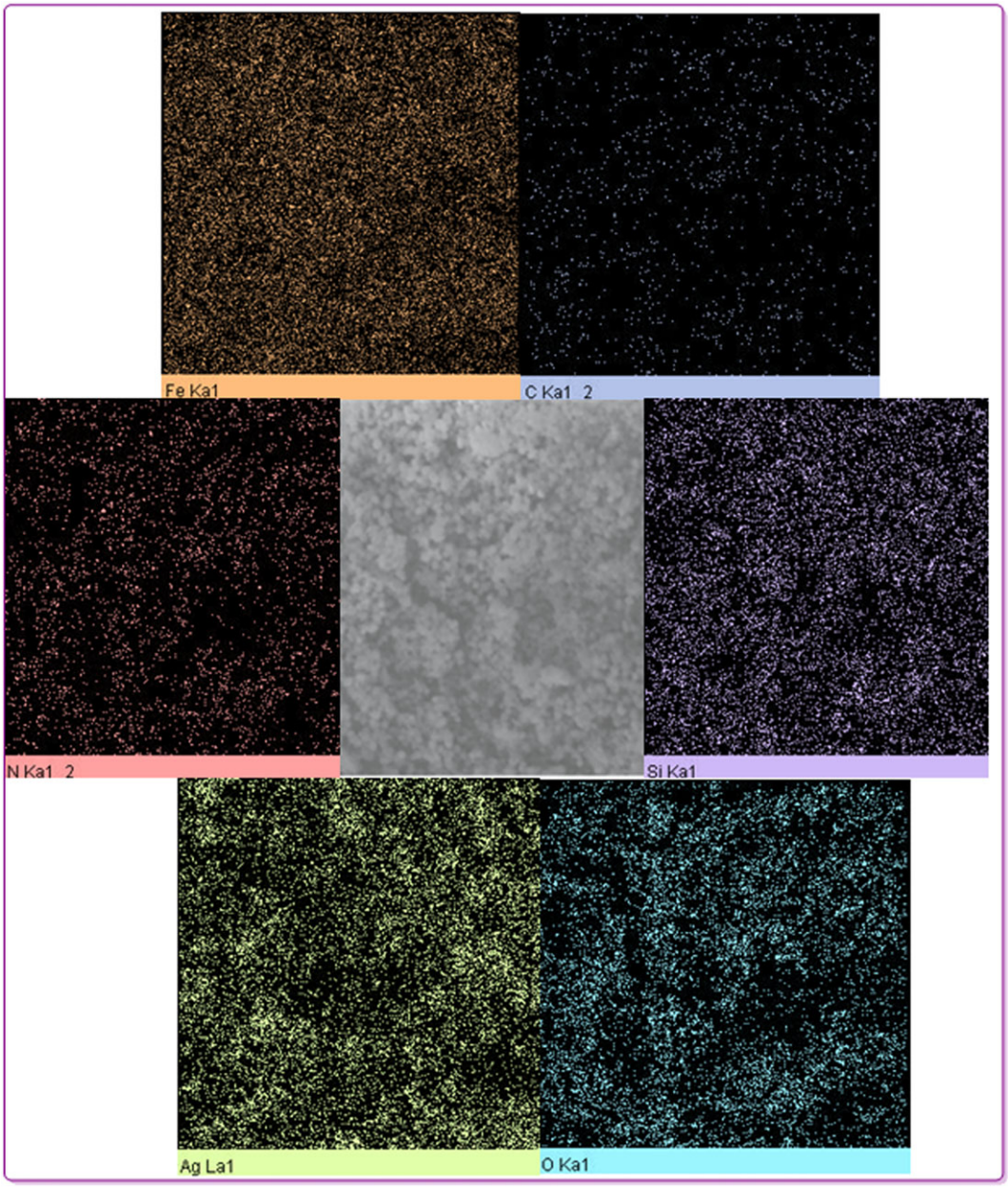

FIGURE 3 Elemental mapping analysis of the catalyst

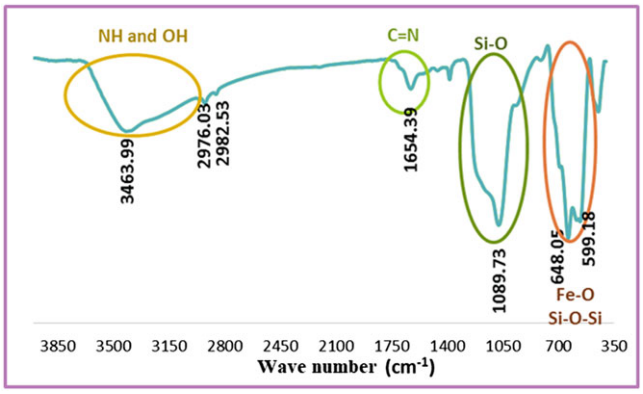

FIGURE 4 FT-IR spectrum of h-Fe_2O_3@SiO_2-IL/Ag

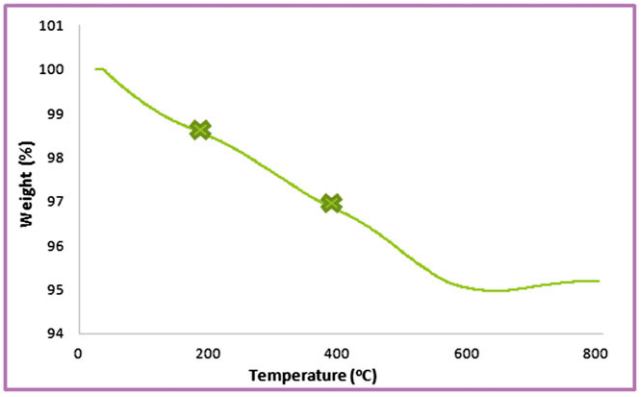

FIGURE 6 TGA analysis of h-Fe_2O_3@SiO_2-IL/Ag

470–590 cm^{-1}.[6] The band at 3463 cm^{-1} is representative of surface hydroxyl groups. Moreover, the bands at 2976 cm^{-1} can be assigned to —CH_2 stretching and is indicative of the presence of IL in the structure of the catalyst. The observed band at 1654 cm^{-1} is assigned to the C═N (imine) functionality and can confirm the conjugation of IL.

The formation of Ag(0) as well as h-Fe_2O_3 was clearly confirmed from the XRD pattern (Figure 5). The peaks at 30.3°, 35.6°, 43.2°, 54.0°, 57.3°, 63.0° and 74.6° (labelled as 'F') are indicative of the {220}, {311}, {400}, {422}, {511}, {440} and {533} planes of the typical cubic structure of hematite (JCPDS card no. 39–1346).[6] The peaks labelled as 'A' are the characteristic peaks of Ag(0) nanoparticles (JCPDS card no. 04–0783). It is worth noting that according to a previous report,[41] the broad halo detected at $2\theta = 5–20°$ (labelled as *) can be due to the formation of amorphous silica and IL. The Debye–Scherrer equation was employed for calculating the average particle size of Ag(0) nanoparticles. This value was determined to be 35 nm.

The thermal stability of h-Fe_2O_3@SiO_2-IL/Ag was investigated using TGA. As shown in Figure 6, h-Fe_2O_3@SiO_2-IL/Ag exhibited two degradation steps over the range 30–800 °C. The initial weight loss (1.4%), occurring below 200 °C, can be assigned to the loss of surface hydroxyl groups and adsorbed water molecules. The weight loss of about 3.5% can be due to the degradation of IL. Hence, the content of organic motif in h-Fe_2O_3@SiO_2-IL/Ag was calculated to be about 3.5 wt%.

ICP-AES analysis was exploited for measuring the content of silver in the catalyst. To prepare a sample for analysis, a known amount of h-Fe_2O_3@SiO_2-IL/Ag was digested in concentrated hydrochloric and nitric acids solution. Then, the obtained extract was analysed using ICP-AES. The silver content was estimated to be 5 wt%.

To elucidate whether decoration of the surface of h-Fe_2O_3 with SiO_2 shell and with IL and Ag(0) nanoparticles can alter the magnetic property, h-Fe_2O_3@SiO_2-IL/Ag was studied at room temperature using VSM, and its magnetic features compared with those of h-Fe_2O_3 (Figure 7). As can be seen, the maximum saturation magnetization (M_s) values of h-Fe_2O_3 and h-Fe_2O_3@SiO_2-IL/Ag are about 45 and 22 emu g^{-1}, respectively. These results indicated that incorporation of non-magnetic component can markedly reduce the magnetic property of h-Fe_2O_3. However, the hysteresis loops of both h-Fe_2O_3 and h-Fe_2O_3@SiO_2-IL/Ag exhibited a superparamagnetic behaviour with their re-dispersion

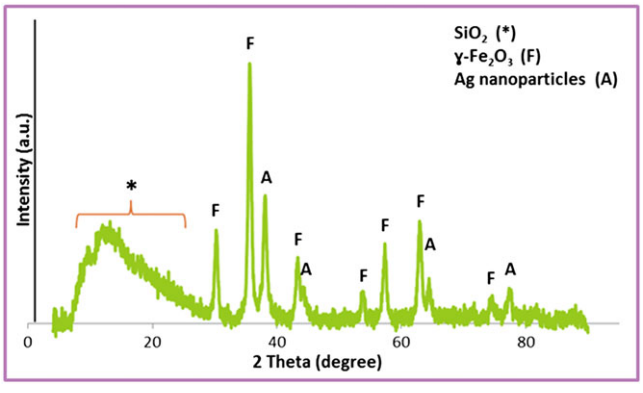

FIGURE 5 XRD pattern of h-Fe_2O_3@SiO_2-IL/Ag

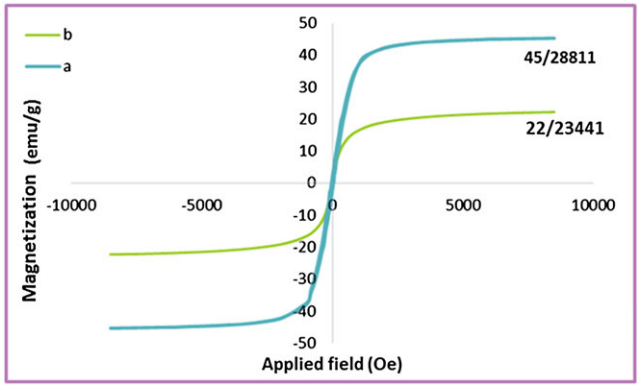

FIGURE 7 VSM analysis of (a) h-Fe_2O_3 and (b) h-Fe_2O_3@SiO_2-IL/Ag

stability in solution, without aggregation. Moreover, no obvious changes in the coercivity from the enlarged view of the central hysteresis loop for h-Fe_2O_3 and h-Fe_2O_3@SiO_2-IL/Ag were observed.

Using BET analysis, the textural features of h-Fe_2O_3@SiO_2-IL/Ag were determined. Figure 8 illustrates the nitrogen adsorption–desorption isotherm of the catalyst. This isotherm, which is of type II with H3 hysteresis loops, clearly confirms the porous structure of the catalyst.[42] The calculated average pore diameter, specific surface area and total pore volume of h-Fe_2O_3@SiO_2-IL/Ag are presented in Table 1.

3.2 | Catalytic activity

Considering the importance of propargylamines and benzo[*b*]furans from the synthetic and biological points of view, the synthesis of propargylamine derivatives from reaction of amines, acetylenes and aldehydes and the synthesis of benzo[*b*]furans through reaction of amines, acetylenes and salicylaldehydes were selected to investigate the catalytic performance of h-Fe_2O_3@SiO_2-IL/Ag. Initially, two model reactions, i.e. reaction of phenylacetylene, benzaldehyde and morpholine and reaction of salicylaldehyde, phenylacetylene and morpholine, were selected to study the necessity of the catalyst and for optimizing the reaction conditions. First, the model reactions were carried out in the absence of the catalyst. The results established that no desired products were obtained in the absence of the catalyst, indicating that the utilization of the catalyst was essential for promoting the reaction and generation of the desired products. Notably, ultrasonic irradiation was selected as an efficient, green and rapid procedure for performing the reactions. A comparison of the yields of the model products under conventional reflux and stirring conditions with those of ultrasonic irradiation clearly established that using ultrasonic irradiation could markedly accelerate the rate of the reaction and improve the yield of the desired products. Interestingly, no by-products were observed under this unconventional condition.

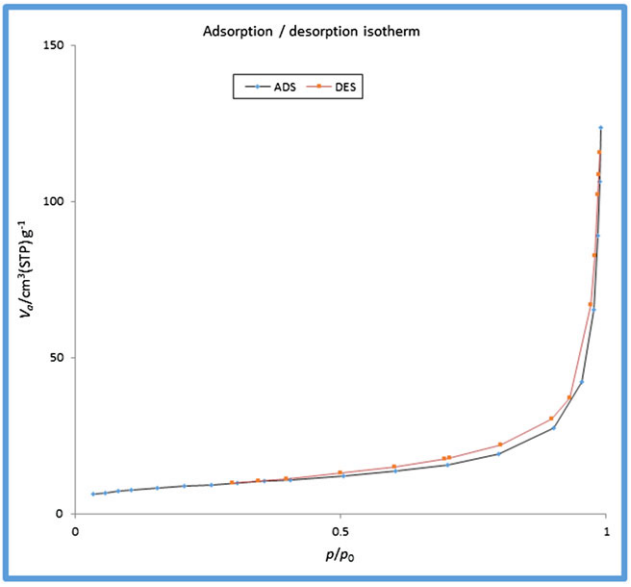

FIGURE 8 Nitrogen adsorption–desorption isotherms of h-Fe_2O_3@SiO_2-IL/Ag

TABLE 1 Textural properties of h-Fe_2O_3@SiO_2-IL/Ag

Catalyst	S_{BET} ($m^2\ g^{-1}$)	Total pore volume ($cm^3\ g^{-1}$)	Average pore diameter (nm)
h-Fe_2O_3@SiO_2-IL/Ag	21	0.18	35

The high efficiency of ultrasonic irradiation was attributed to the cavitation phenomenon.[31,43] This phenomenon includes generation, growth and collapse of cavities. This can cause high local temperatures and pressures and focus vert large amounts of energy from the conversion of kinetic energy of liquid motion into heating of the contents of the cavities.[43]

Then, the reaction conditions were optimized for both model reactions. For this purpose, the yields of the model products on altering the reaction variables such as solvent, power of ultrasonic irradiation and catalyst amount were compared. In Figure 9, the results for optimization of the model synthesis of propargylamine are depicted. As shown, the best results were obtained using water as a green solvent. In this solvent, increasing the amount of the catalyst from 15 to 25 mg had a positive effect on the yield of the product. However, further increase in this value had no significant effect on the yield of the product. Moreover, increasing the power of ultrasonic irradiation from 50 to 100 W improved the yield of the reaction. However, this trend was not steady and a further increase in power did not alter the yield of the product. Hence, performing the reaction in water in the presence of

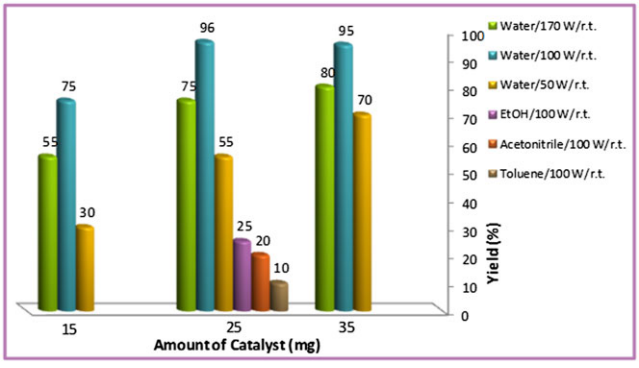

FIGURE 9 Effects of loading of catalyst, duration of reaction and solvent for the synthesis of propargylamine

25 mg of the catalyst and using an ultrasonic irradiation of power 100 W were found to be the optimum reaction conditions. Similarly, the reaction conditions for the synthesis of benzo[*b*]furan were optimized. The optimum reaction variables for this reaction were using 25 mg of the catalyst, an ultrasonic irradiation of power of 100 W and water as solvent.

Armed with the optimum reaction conditions, the generality of these two protocols was investigated using various aromatic and aliphatic aldehydes, acetylenes and amines with various electron densities and steric features (Tables 2 and 3). Gratifyingly, all amines, acetylenes and aldehydes could be successfully used in these protocols to furnish the corresponding products in excellent yields in very short reaction times.

Next, to elucidate the merit of h-Fe_2O_3@SiO_2-IL/Ag catalyst and ultrasonic irradiation, the performance of h-Fe_2O_3@SiO_2-IL/Ag for the model synthesis of propargylamine was compared with that of some of previously reported catalysts (Table 4). As is evident, using ultrasonic irradiation could markedly accelerate the reaction rate. Notably, bare h-Fe_2O_3 exhibited a catalytic activity to some extent. However, the performance of h-Fe_2O_3@SiO_2-IL/Ag is superior compared to h-Fe_2O_3, indicating the role of silver nanoparticles in the catalytic cycle. The h-Fe_2O_3@SiO_2-IL/Ag catalyst exhibited catalytic performance comparable to our previously reported magnetic catalyst,[6] h-Fe_2O_3@DA/Ag, implying the efficiency of hybrid magnetic catalysts based on a combination of h-Fe_2O_3 and silver nanoparticles. Compared to other catalysts presented in Table 4, h-Fe_2O_3@SiO_2-IL/Ag showed higher or comparable catalytic activity. Moreover, this catalyst could promote the reaction at room temperature in water with no need for inert conditions. Hence, this protocol can be considered as a mild, green and rapid strategy. Although Table 4 does not include all the catalysts used for the synthesis of model propargylamine, this comparison can demonstrate the advantageous catalytic activity of h-Fe_2O_3@SiO_2-IL/Ag.

3.3 | Reaction mechanism

Based on previous reports,[44,45] a possible reaction mechanism for the synthesis of propargylamines includes initial activation of the terminal C—H bond of acetylene by h-Fe_2O_3@SiO_2-IL/Ag and subsequent generation of silver acetylide intermediate. The catalyst can also promote the formation of imnium ion through the reaction of amine and aldehyde. Then, the generated imnium ion undergoes reaction with silver acetylide to afford the corresponding propargylamine as well as h-Fe_2O_3@SiO_2-IL/Ag (Scheme 2).

Regarding the reaction mechanism for the formation of benzofurans,[28] it is speculated that the catalyst induces generation of silver acetylide intermediate which then undergoes reaction with iminium ion that is produced *in situ* through the reaction of salicylaldehyde and amine. h-Fe_2O_3@SiO_2-IL/Ag can also act as a Lewis acid and catalyse a cyclization reaction via nucleophilic attack by hydroxyl group to furnish the desired product and the catalyst.

3.4 | Catalyst reusability

Considering the importance of simple recovery and reusability of heterogeneous catalysts, the reusability of h-Fe_2O_3@SiO_2-IL/Ag for the model synthesis of propargylamine and benzo[*b*]furan was investigated. For this purpose, the catalyst was recovered after the first reaction run using an external magnet. The recovered catalyst was washed with EtOH, dried and subjected to the next reaction run. The reusability of the catalyst was studied for seven successive runs and the yields of the products obtained using fresh and recycled catalysis were compared (Figure 10). As is obvious, for both reactions, the catalyst could be successfully reused with only slight loss of catalytic activity. Next, to establish the stability of the reused catalyst, the FT-IR spectrum of fresh h-Fe_2O_3@SiO_2-IL/Ag was compared with that of the reused one (Figure 11). Both fresh and reused catalyst exhibited similar bands in their FT-IR spectra, implying that the catalyst preserved its structure upon reuse.

Finally, to study the nature of the catalysis and the leaching of Ag(0) nanoparticles, ICP-AES analysis of the reused catalyst was performed. Interestingly, the results established almost zero leaching of Ag(0) nanoparticles, indicating the heterogeneous nature of the catalysis and the efficiency of immobilized IL for anchoring Ag(0) nanoparticles on h-Fe_2O_3@SiO_2.

3.5 | Spectral data for some selected compounds, Supporting information

1-(1,3-Diphenylprop-2-ynyl)piperidine (Table 2, 6a). Pale yellow oily liquid. ^{1}H NMR (400 MHz, $CDCl_3$, δ, ppm): 1.45–1.49 (m, 2H), 1.58–1.65 (m, 4H), 2.59 (t, 4H), 4.81 (s, 1H), 7.31–7.40 (m, 6H), 7.53–7.55 (m, 2H), 7.65–7.67 (d, J = 7.6 Hz, 2H).

1-(3-Phenyl-1-(4-(3-phenyl-1-(piperidin-1-yl)prop-2-ynyl)phenyl)prop-2-ynyl)piperidine (Table 2, 6 h). White solid; m.p. 157–159 °C (lit.[46] 158–160 °C). ^{1}H NMR (400 MHz, $CDCl_3$, δ, ppm): 1.47 (m, 2H), 1.59–1.63 (m, 4H), 2.59 (m, 4H), 4.81 (s, 1H), 7.33–7.35 (m, 3H), 7.52–7.55 (m, 2H), 7.63 (s, 2H).

TABLE 2 Synthesis of three-component reaction of aldehyde or cyclic ketone, secondary amine and terminal alkyne catalysed by h-Fe_2O_3@SiO_2-IL/Ag[a][9,28,44–48]

R_1	R_2	R_3	R_4	R_5	Product	Time (min)	Yield (%)[b]
1a: C_6H_5	H	4a: —$(CH_2)_5$—		5a: C_6H_5	**6a**	10	92
1b: *p*-cl-C_6H_4	H	4a		5a	**6b**	10	92
1c: *p*-NO_2-C_6H_4	H	4a		5a	**6c**	15	95
1d: *p*-me-C_6H_4	H	4a		5a	**6d**	18	92
1e: *p*-MeO-C_6H_4	H	4a		5a	**6e**	10	90
1f: *o*-OH-C_6H_4	H	4a		5a	**6f**	8	94
1g: Furfuryl	H	4a		5a	**6g**	15	80
1h: *p*-OHCC_6H_4	H	4a		5a	**6h**	10	90
1i: *o*-Naphthyl	H	4a		5a	**6i**	15	92
1a	H	4a		5b: *p*-CH_3_C_6H_4	**6j**	18	90
1a	H	4a		5c: *p*-F-C_6H_4	**6k**	20	88
1a	H	4b: —$(CH_2)_2O(CH_2)_2$—		5a	**6l**	10	96
1b	H	4b		5a	**6m**	15	85
1c	H	4b		5a	**6n**	15	82
1d	H	4b		5a	**6o**	15	90
1e	H	4b		5a	**6p**	10	90
1f	H	4b		5a	**6q**	17	90
1g	H	4b		5a	**6r**	25	91
1j: *m*-NO_2-C_6H_4	H	4b		5a	**6s**	30	92
1a	H	4b		5b	**6t**	15	90
1a	H	4c: —$(CH_2)_4$—		5a	**6u**	15	93
1a	H	4d: C_2H_5	C_2H_5	5a	**6v**	13	82
2a[c]: H	H	4a		5a	**7a**	8	92
2a	H	4a		5b	**7b**	10	86
2a	H	4b		5a	**7c**	10	91
2a	H	4c		5a	**7d**	10	90
2a	H	4d		5a	**7e**	15	82
2b: C_6H_{11}	H	4a		5a	**7f**	15	92
2b	H	4b		5b	**7g**	17	85
2b	H	4b		5a	**7h**	13	90
2b	H	4c		5a	**7i**	15	83
2b	H	4d		5a	**7j**	19	79
2c: —$(CH_2)_2$—me	H	4a		5a	**7l**	15	91
2c	H	4b		5a	**7m**	10	85
2c	H	4c		5a	**7n**	19	82
2c	H	4d		5a	**7o**	20	80
3a: —$(CH_2)_4$—		4a		5a	**8a**	20	88
3a		4b		5a	**8b**	22	90
3a		4c		5a	**8c**	22	91
3b: —$(CH_2)_5$—		4a		5a	**8d**	25	92

(Continues)

TABLE 2 (Continued)

R_1	R_2	R_3	R_4	R_5	Product	Time (min)	Yield (%)[b]
3b		4a		5b	**8e**	30	89
3b		4b		5a	**8f**	33	88
3b		4b		5b	**8g**	35	85
3b		4b		5c	**8h**	28	90
3b		4c		5a	**8i**	23	92

[a]Reaction conditions: arylaldehydes **1a–j** (1.0 equiv.) or aliphatic aldehyde **2a–c** (1.0 equiv.) or aliphatic ketone **3a**, **b** (1.0 equiv.),amines **4a–d** (1.0 equiv.), alkynes **5a–c** (1.1 equiv.), H_2O (20 ml) and h-Fe_2O_3@SiO_2-IL/Ag (0.025 g) under ultrasonic irradiation (100 W) at room temperature.

[b]Isolated yield.

[c]Aqueous formaldehyde (37%, 0.4 ml).

TABLE 3 Synthesis of three-component reaction of salicylaldehyde, secondary amine and terminal alkyne catalysed by h-Fe_2O_3@SiO_2-IL/Ag[a]

R_6	R_3 R_4	R_5	Product	Time (min)	Yield (%)[b]	Ref.
9a: H	**3a**: —$(CH_2)_5$—	**5a**	**10a**	40	90	[28]
9b: Br	**3a**	**5a**	**10b**	35	92	[28]
9c: NO_2	**3a**	**5a**	**10c**	30	93	[30]
9a	**3b**: —$(CH_2)_2O(CH_2)_2$—	**5a**	**10d**	30	85	[28]
9a	**3b**	**5c**	**10e**	30	88	[30]
9b	**3b**	**5a**	**10f**	25	88	[28]
9c	**3b**	**5a**	**10 g**	20	90	[30]
9c	**3b**	**5b**	**10 h**	30	91	[30]

[a]Reaction conditions: arylaldehydes **1a** (1.0 equiv.) or aliphatic ketone **2a** (1.0 equiv.), amines **3a** (1.0 equiv.), alkynes (1.1 equiv.), H_2O (20 ml) and h-Fe_2O_3@SiO_2-IL/Ag(0.025 g) under ultrasonic irradiation (100 W) at room temperature.

[b]Isolated yield.

TABLE 4 Comparison of h-Fe_2O_3@SiO_2-IL/ag with other recently reported acid catalysts for synthesis of propargylamines (Scheme 1)

Catalyst	Reaction conditions	Time (min)	Catalyst amount	Yield (%)	Ref.
h-Fe_2O_3@SiO_2-IL/Ag	H_2O/ r.t./ultrasound	12	25 mg	96	This work
h-Fe_2O_3@DA/Ag	Sf/90 °C	60	10 mg	96	[6]
h-Fe_2O_3	H_2O/r.t./ultrasound	12	25 mg	75	This work
ZnO nanoparticles	Stirrer/90 °C	120	10 mol%	89	[13]
Immobilized silver on surface-modified ZnO nanoparticles	Reflux/H_2O	240	10 mol%	89	[52]
Ag-CIN-1[a]	H_2O/40 °C	720	5 mg	65	[49]
Ag^I-pc-L[b]	Toluene/MW/150 °C	20	3 mol%	59	[50]
CuNPs/TiO_2	Neat/70 °C	420	0.5 mol%	91	[10]
ZnS	Reflux/CH_3CN	270	10 mol%	89	[51]
Sulfonate-based cu(I) metal–organic frameworks	Reflux/EtOH, 90 °C	1440	20 mg	87	[17]
CuI catalysts supported on protonated trititanate nanotubes	Solvent-free, 70 °C	90	20 mg	95	[20]
Cu_2O/nano-$CuFe_2O_4$	Solvent-free, 90 °C	40	10 mg	93	[18]
Copper nanoparticles supported on starch microparticles	THF, 60 °C	1200	0.3 mol%	95	[21]
Cu(II) Schiff base complex immobilized on graphene oxide	Water, reflux, N_2	900	20 mg	83	[19]

[a]Ag-grafted covalent imine network material.

[b]Ag(I)–(pyridine-containing ligand) complexes.

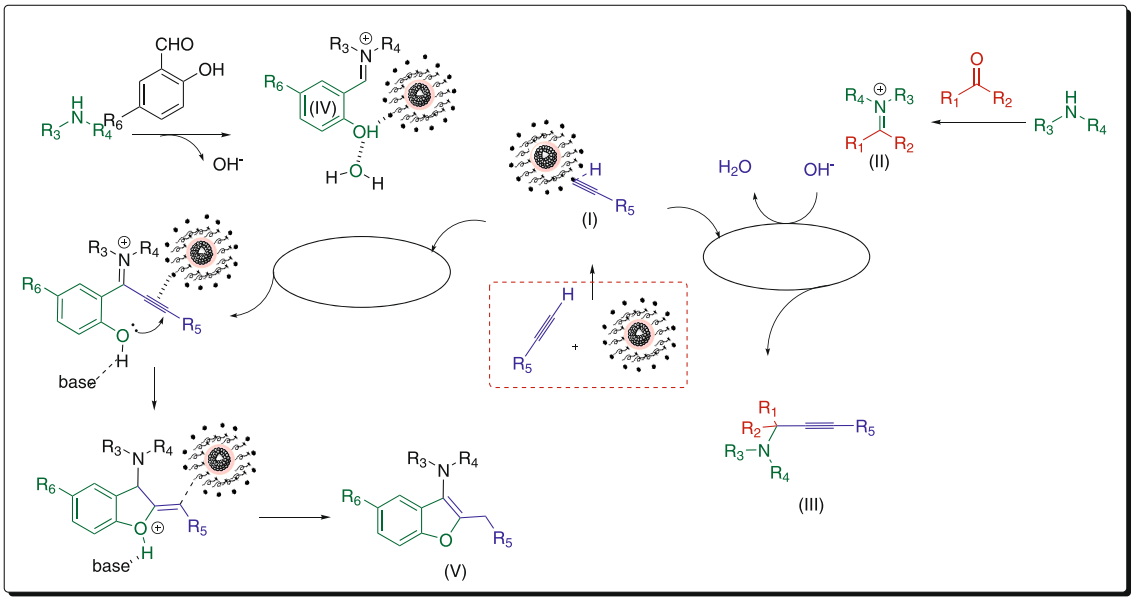

SCHEME 2 Plausible mechanism for synthesis of propargylamines and benzo[*b*]furans catalysed by h-Fe_2O_3@SiO_2-IL/Ag

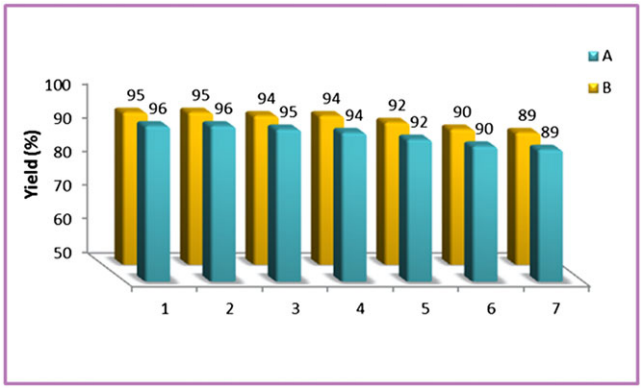

FIGURE 10 Reusability of h-Fe_2O_3@SiO_2-IL/Ag catalyst for synthesis of (a) propargylamine and (b) benzofuran

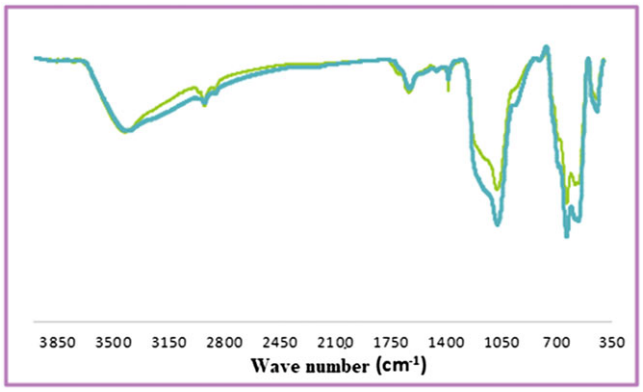

FIGURE 11 Comparison of FT-IR spectra of fresh h-Fe_2O_3@SiO_2-IL/Ag and after seven runs

1-(1-(Naphthalen-3-yl)-3-phenylprop-2-ynyl)piperidine (Table 2, 6i). Yellow oil. ^{1}H NMR (400 MHz, $CDCl_3$, δ, ppm): 1.47–1.51 (m, 2H), 1.60–1.67 (m, 4H), 2.64 (t, 4H), 4.97 (s, 1H), 7.36–7.40 (m, 3H), 7.48–7.52 (m, 2H), 7.58–7.61 (m, 2H), 7.79 (dd, $J^1 = J^2 = 8.4$ Hz, 1H), 7.85–7.91 (m, 3H), 8.11 (s, 1H). ^{13}C NMR (100 MHz, $CDCl_3$, δ, ppm): 24.4, 26.2, 50.8, 62.5, 86, 88.1, 123.3, 125.8, 125.9, 126.7, 127.2, 127.5, 127.7, 128.1, 128.12, 131.8, 132.9, 133.1, 136.3.

N,*N*-Diethyl-1,3-diphenylprop-2-yn-1-amine (Table 2, 6v). Pale yellow oily liquid. ^{1}H NMR (400 MHz, $CDCl_3$, δ, ppm): 1.04 (m, 6H), 2.36–2.62 (m, 4H), 5.19 (s, 1H), 7.15–7.27 (m, 4H), 7.29–7.38 (m, 3H), 7.39–7.41 (m, 2H).

4-(3-Phenylprop-2-ynyl)morpholine (Table 2, 7c). Yellow oil. ^{1}H NMR (400 MHz, $CDCl_3$, δ, ppm): 2.64–2.67 (m, 6H), 3.52 (s, 3H), 3.69–3.71 (m, 1H), 3.77–3.79 (m, 6H), 7.28–7.31 (m, 4H), 7.43–7.46 (m, 2H).

1-(1-Cyclohexyl-3-phenylprop-2-ynyl)pyrrolidine (Table 2, 7i), Colourless liquid. ^{1}H NMR (400 MHz, $CDCl_3$, δ, ppm): 1.05–1.36 (m, 5H), 1.56–1.63 (m, 2H), 1.75–1.79 (m, 6H), 1.82–2.10 (m, 4H), 2.5–2.98 (m, 4H), 3.36–3.38 (d, J = 7.6 Hz, 1H), 7.14–7.33 (m, 3H), 7.50–7.63 (m, 2H). ^{13}C NMR (100 MHz, $CDCl_3$, δ, ppm): 24.9, 26.9, 27.1, 28.3, 32.7, 33, 42.9, 51.1, 61.1, 86.1, 88.9, 125.9, 128.9, 129.8, 132.6.

4-(1-Phenylhex-1-yn-3-yl)morpholine (Table 2, 7 m). Yellow oil. ^{1}H NMR (400 MHz, DMSO-d_6, δ, ppm): 0.97 (m, 3H), 1.45–1.75 (m, 4H), 2.67–2.70 (m, 2H), 2.79–2.83 (m, 2H), 3.82–4.13 (m, 1H), 4.15–4.17 (m, 4H), 7.46–7.50 (m, 3H), 7.62–7.64 (m, 2H).

4-(1-(2-Phenylethynyl)cyclohexyl)morpholine(Table 2, 8f). Pale yellow oily liquid. ^{1}H NMR (400 MHz, $CDCl_3$, δ, ppm): 1.28–1.30 (m, 1H), 1.52 (m, 2H), 1.63–1.67 (m, 3H), 1.73 (br.s, 2H), 2.03–2.05 (m, 2H), 2.74 (br.s, 4H), 3.78 (br. s, 4H), 7.27 (m, 3H), 7.44–7.45 (m, 2H). ^{13}C NMR (100 MHz, $CDCl_3$, δ, ppm): 22.7, 25.7, 35.4, 46.6, 58.8, 67.4, 86.4, 89.8, 123.4, 127.7, 128.1, 131.7.

4-(1-((4-Fluorophenyl)ethynyl)cyclohexyl)morpholine (Table 2, 8 h). Yellow oil. ^{1}H NMR (400 MHz, DMSO-d_6, δ, ppm): 1.26–1.34 (m, 1H), 1.57–1.62 (m, 2H), 1.69–1.78 (m, 3H), 1.80–1.86 (m, 2H), 2.00–2.02 (m, 2H), 2.78 (s, 4H), 3.70 (br.t, J = 4.2 Hz, 4H), 6.97–7.00 (t, J = 8.6 Hz, 2H), 7.32–7.40 (m, 2H).

4-(2-Benzylbenzofuran-3-yl)morpholine (Table 3, **10d**). Yellow solid, m.p. 107–109 °C (lit.[28] 106–108 °C). ^{1}H NMR (400 MHz, $CDCl_3$, δ, ppm): 3.19 (t, J = 4.5 Hz, 4H, 2 CH_2-N), 3.87 (t, J = 4.5 Hz, 4H, 2CH_2-O), 4.20 (s, 2H, CH_2), 7.19–7.34 (m, 7H, ArH), 7.40–7.42 (d, J = 8 Hz, 1H, ArH), 7.69–7.71 (d, J = 8 Hz, 1H, ArH). ^{13}C NMR (100 MHz, $CDCl_3$, δ, ppm): 31.4, 51.7, 67.0, 112.7, 114.7, 121.5, 125.6, 126.3, 127.6, 127.8, 128.0, 128.2, 137.1, 150.8, 152.1.

4-(2-Benzyl-5-bromobenzofuran-3-yl)morpholine (Table 3, **10f**). Yellow solid, m.p. 110–112 °C (lit.[28] 110–111 °C). ^{1}H NMR (400 MHz, $CDCl_3$, δ, ppm): 3.14 (t, J = 5 Hz, 4H, 2 CH_2-N), 3.85 (t, J = 5 Hz, 4H, 2CH_2-O), 4.16 (s, 2H, CH_2), 7.21–7.53 (m, 8H, ArH), 7.79 (s, 1H, ArH). ^{13}C NMR (100 MHz, $CDCl_3$, δ, ppm): 32.3, 52.4, 67.6, 113.1, 115.2, 122.4, 126.3, 126.6, 128.0, 128.2, 128.5, 128.6, 137.3, 151.7, 152.2.

4-(2-Benzyl-5-nitrobenzofuran-3-yl)morpholine (Table 3, **10 g**). Yellow solid, m.p. 118–120 °C (lit.[30] 118–120 °C). ^{1}H NMR (400 MHz, $CDCl_3$, δ, ppm): 3.19 (t, J = 4.8 Hz, 4H, 2 CH_2-N), 3.87 (t, J = 4.8 Hz, 4H, 2CH_2-O), 4.21 (s, 2H, CH_2), 7.27–7.35 (m, 5H, ArH), 7.43–7.45 (d, J = 10 Hz, 1H, ArH), 8.14–8.17 (d, J = 10 Hz, 1H, ArH), 8.57 (s, 1H, ArH). ^{13}C NMR (100 MHz, $CDCl_3$, δ, ppm): 32.5, 53.1, 68.5, 113.1, 114.6, 122.7, 125.1, 126.5, 127.1, 127.3, 128.1, 128.3, 138.8, 150.7, 151.1.

4-(2-(4-Methylbenzyl)-5-nitrobenzofuran-3-yl)morpholine (Table 3, **10 h**). Yellow solid; m.p. 107–109 °C (lit.[30] 107.1–107.9 °C). ^{1}H NMR (400 MHz, $CDCl_3$, δ, ppm): 2.32 (s, 3H), 3.18 (t, J = 4.5 Hz, 4H), 3.88 (t, J = 4.5 Hz, 4H), 4.15 (s, 2H), 7.16–7.11 (m, 4H), 7.42 (d, J = 8.3 Hz, 1H), 8.13 (d, J = 9.1 Hz, 1H), 8.54 (s, 1H). ^{13}C NMR (100 MHz, $CDCl_3$, δ, ppm): 21.1, 32.2, 52.5, 67.6, 112.01, 116.3, 119.64, 126.6, 128.5, 129.4, 129.5, 134.1, 136.63, 143.5, 153.83, 156.35.

4 | CONCLUSIONS

For the first time, a hybrid magnetic hybrid catalyst, h-Fe_2O_3@SiO_2-IL/Ag, was designed and synthesized through incorporation of [pmim]Cl with h-Fe_2O_3@SiO_2 and subsequent immobilization of silver nanoparticles via a biosynthetic approach. The contents of silver and organic moiety in the final catalyst were estimated to be 5 and 3.5 wt%, respectively. The catalytic activity of h-Fe_2O_3@SiO_2-IL/Ag for catalysing green and ultrasonic-assisted A^3 and KA^2 coupling reactions as well as benzo[*b*]furan synthesis was confirmed. Reusability studies confirmed that the magnetic catalyst could be easily separated from the reaction mixture and reused for seven reaction runs with only slight loss of catalytic activity. ICP-AES analysis confirmed suppressed silver leaching and proved the heterogeneous nature of the catalysis. High yields, short reaction times, broad substrate scope and low amount of catalyst are other advantages of this methodology. Moreover, using aqueous media and ultrasonic irradiation rendered this protocol green and environmentally friendly.

ACKNOWLEDGEMENTS

The authors are grateful for partial financial support from Alzahra University and Iran Polymer and Petrochemical Institute. M.M.H. is also grateful to Iran National Science Foundation for an individual grant.

ORCID

Samahe Sadjadi http://orcid.org/0000-0002-6884-4328
Majid M. Heravi http://orcid.org/0000-0003-2978-1157

REFERENCES

[1] X. Zhang, Y. Niu, Y. Yang, Y. Li, J. Zhao, *New J. Chem.* **2014**, *38*, 4351.

[2] N. E. A. El-Gamel, L. Wortmann, K. Arroubb, S. Mathur, *Chem. Commun.* **2011**, *47*, 10076.

[3] T. Georgelin, V. Maurice, B. Malezieux, J.-M. Siaugue, V. Cabuil, *J. Nanopart. Res.* **2010**, *12*, 675.

[4] S. Meng, H. Wang, M. Qing, C. Qiu, Y. Yang, L. Y. Li, *J. Fuel Chem. Technol.* **2015**, *43*, 692.

[5] J. Zhu, Y. Shen, C. Yao, A. Xie, *Colloid J.* **2016**, *78*, 156.

[6] A. Elhampour, E. Malmir, M. Kowsari, F. A. Boorboor, F. Nemati, *RSC Adv.* **2016**, *6*, 96623.

[7] Q. He, Z. Wu, C. Huang, *J. Nanosci. Nanotechnol.* **2012**, *12*, 2943.

[8] Y. Gu, *Green Chem.* **2012**, *14*, 2091.

[9] S. V. Katkar, R. V. Jayaram, *RSC Adv.* **2014**, *4*, 47958.

[10] M. J. Albaladejo, F. Alonso, Y. Moglie, M. Yus, *Eur. J. Org. Chem.* **2012**, 3093.

[11] G. Villaverde, A. Corma, M. Iglesias, F. Sanchez, *ACS Catal.* **2012**, *2*, 399.

[12] N. Salam, S. K. Kundu, A. Singha Roy, P. Mondal, S. Roy, A. Bhaumik, S. Manirul Islam, *Cat. Sci. Technol.* **2013**, *3*, 3303.

[13] K. V. V. Satyanarayana, P. Atchuta Ramaiah, Y. L. N. Murty, M. R. Chandra, S. V. N. Pammi, *Cat. Com.* **2012**, *25*, 50.

[14] B. J. Borah, S. J. Borah, K. L. Saikia, D. K. Dutta, *Cat. Sci. Technol.* **2014**, *4*, 4001.

[15] T. Zeng, W.-W. Chen, C. M. Cirtiu, A. Moores, G. Song, C.-J. Li, *Green Chem.* **2010**, *12*, 570.

[16] T.-W. Hui, J.-F. Cui, M.-K. Wong, *RSC Adv.* **2017**, *7*, 14477.

[17] P. Li, S. Regati, H.-C. Huang, H. D. Arman, B.-L. Chen, J. C.-G. Zhao, *Chin. Chem. Lett.* **2015**, *26*, 6.

[18] F. Nemati, A. Elhampour, H. Farrokhi, M. Bagheri Natanzi, *Cat. Com.* **2015**, *66*, 15.

[19] S. Kumari, A. Shekhar, D. D. Pathak, *RSC Adv.* **2016**, *6*, 15340.

[20] B. R. Prasad Reddy, P. V. Govardhana Reddy, M. V. Shankar, B. N. Reddy, *Asian J. Org. Chem.* **2017**, *6*, 712.

[21] M. Gholinejad, F. Saadati, S. Shaybanizadeh, B. Pullithadathil, *RSC Adv.* **2016**, *6*, 4983.

[22] Z. L. Palchak, D. J. Lussier, C. J. Pierce, C. H. Larsen, *Green Chem.* **2015**, *17*, 1802.

[23] A. M. Munshi, M. Shi, S. P. Thomas, M. Saunders, M. A. Spackman, K. S. Iyer, N. M. Smith, *Dalton Trans.* **2017**, *46*, 5133.

[24] M. Mirabedini, E. Motamedi, M. Z. Kassaee, *Chin. Chem. Lett.* **2015**, *26*, 1085.

[25] G.-P. Yong, D. Tian, H.-W. Tong, S.-M. Liu, *J. Mol. Catal. A* **2010**, *323*, 40.

[26] T. J. Simpson, R. H. Thomson, *The Chemistry of Natural Products*, Blackie, London **1985**.

[27] J. Li, T. S. Rush, D. Vincentis, J. S. Skotnicki, S. Tam, K. M. Cunningham, *Bioorg. Med. Chem. Lett.* **2005**, *15*, 4961.

[28] J. Safaei-Ghomi, M. A. Ghasemzadeh, A. Kakavand-Qalenoei, *J. Saudi Chem. Soc.* **2016**, *20*, 502.

[29] D. Das, *Chem. Select* **2016**, *1*, 1959.

[30] G. Purohit, U. C. Rajesh, D. S. Rawat, *ACS Sustain. Chem. Eng.* **2017**, *5*, 6466.

[31] H. Naeimi, R. Shaabani, *Ultrason. Sonochem.* **2017**, *34*, 246.

[32] M. Navid, S. Rad, *Ultrason. Sonochem.* **2017**, *34*, 865.

[33] M. M. Heravi, F. Mousavizadeh, N. Ghobadi, M. Tajbakhsh, *Tetrahedron Lett.* **2014**, *55*, 1226.

[34] S. Sadjadi, M. M. Heravi, M. Daraie, *J. Mol. Liq.* **2017**, *231*, 98.

[35] S. Sadjad, M. M. Heravi, M. Daraie, *Res. Chem. Intermed.* **2017**, *43*, 843.

[36] S. Sadjadi, M. M. Heravi, M. Daraie, *Res. Chem. Intermed.* **2017**, *43*, 2201.

[37] T. B. Lashaki, H. A. Oskooie, T. Hosseinnejad, M. M. Heravi, *J. Coord. Chem.* **2017**, *70*, 1815.

[38] S. Sadjadi, M. M. Heravi, V. Zadsirjan, M. Ebrahimzadeh, *Res. Chem. Intermed.* (in press).

[39] T. K. H. Ta, M.-T. Trinh, N. V. Long, T. T. M. Nguyen, T. L. T. Nguyen, T. L. Thuoc, B. T. Phan, D. Mott, S. Maenosono, H. Tran-Van, V. H. Le, *Colloids Surf., A* **2016**, *504*, 1.

[40] J. Xiong, W. Zhu, W. Ding, L. Yang, Y. Chao, H. Li, F. Zhu, H. Li, *Ind. Eng. Chem. Res.* **2014**, *53*, 19895.

[41] C. Cannas, A. Musinu, G. Navarra, G. Piccaluga, *Phys. Chem. Chem. Phys.* **2004**, *6*, 3530.

[42] P. Yuan, P. D. Southon, Z. Liu, M. E. R. Green, J. M. Hook, S. J. Antill, C. J. Kepert, *J. Phys. Chem. C* **2008**, *112*, 15742.

[43] S. Sadjadi, M. Eskandari, *Ultrason. Sonochem.* **2013**, *20*, 640.

[44] L. Shi, Y.-Q. Tu, M. Wang, F.-M. Zhang, C.-A. Fan, *Org. Lett.* **2004**, *6*, 1001.

[45] A. Elhampour, M. Malmir, E. Kowsari, F. Boorboor ajdari, F. Nemati, *RSC Adv.* **2016**, *6*, 96623.

[46] M. Tajbakhsh, M. Farhang, S. M. Baghbanian, R. Hosseinzadeh, M. Tajbakhsh, *New J. Chem.* **2015**, *39*, 1827.

[47] M. S. Hosseini, F. Moeini, *New J. Chem.* **2014**, *38*, 624.

[48] M. Tajbaksh, M. Farhang, H. R. Mardani, R. Hosseinzadeh, Y. Sarrafi, *Chin. J. Catal.* **2013**, *34*, 2217.

[49] N. Salam, S. K. Kundu, R. A. Molla, P. Mondal, A. Bhaumik, S. M. Islam, *RSC Adv.* **2014**, *4*, 47593.

[50] M. Trose, M. Dell'Acqua, T. Pedrazzini, V. Pirovano, E. Gallo, E. Rossi, A. Caselli, G. Abbiati, *J. Org. Chem.* **2014**, *79*, 7311.

[51] N. P. Eagalapati, A. Rajack, Y. L. N. Murthy, *J. Mol. Catal. A* **2014**, *381*, 126.

[52] F. Movahedia, H. Masrouria, M. Z. Kassaee, *J. Mol. Catal. A* **2014**, *395*, 52.

SUPPORTING INFORMATION

Additional Supporting Information may be found online in the supporting information tab for this article.

How to cite this article: Sadjadi S, Heravi MM, Malmir M. Green bio-based synthesis of Fe_2O_3@SiO_2-IL/Ag hollow spheres and their catalytic utility for ultrasonic-assisted synthesis of propargylamines and benzo[*b*]furans. *Appl Organometal Chem*. 2017;e4029. https://doi.org/10.1002/aoc.4029